



Preparation of Ag@Ag₃PO₄@ZnO ternary heterostructures for photocatalytic studies



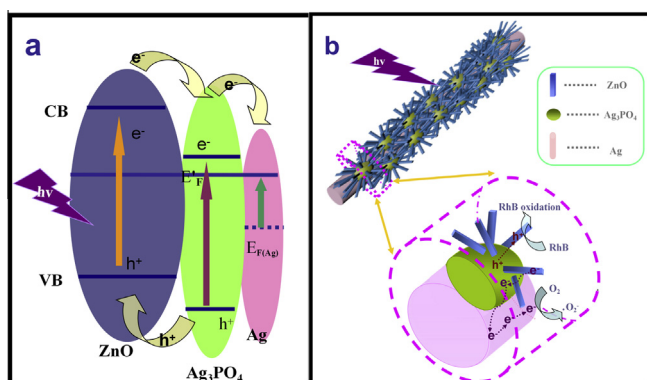
Chao Jin^a, Guanglei Liu^a, Lianhai Zu^a, Yao Qin^{b,c,*}, Jinhu Yang^{a,b,*}

^a Department of Chemistry, Tongji University, Siping Road 1239, Shanghai 200092, People's Republic of China

^b Research Center for Translational Medicine, East Hospital, Tongji University School of Medicine, Tongji University, No. 150 Jimo Road, Shanghai 200120, People's Republic of China

^c Key Laboratory of Arrhythmias of the Ministry of Education of China, East Hospital, Tongji University School of Medicine, No. 150 Jimo Road, Shanghai 200120, People's Republic of China

GRAPHICAL ABSTRACT



ARTICLE INFO

Article history:

Received 7 November 2014

Accepted 28 March 2015

Available online 30 April 2015

Keywords:

Ag@Ag₃PO₄@ZnO

Ternary heterostructures

1D core-shell

Photocatalysis

ABSTRACT

In this article, we report a novel Ag@Ag₃PO₄@ZnO ternary heterostructures synthesized through a three-step approach. Firstly, single-crystalline Ag nanorods are fabricated and served as the templates for subsequent Ag₃PO₄ deposition. Secondly, Ag₃PO₄ crystals are grown around Ag core nanorods through a solution co-precipitation process, leading to the Ag@Ag₃PO₄ binary heterostructures. Finally, ZnO nanorod arrays on the surface of the Ag@Ag₃PO₄@ZnO ternary heterostructures are realized via a seeded growth strategy, forming the typical Ag@Ag₃PO₄@ZnO ternary heterostructures. The photodegradation of rhodamine B under ultraviolet–visible light irradiation indicates that the Ag@Ag₃PO₄@ZnO ternary heterostructures exhibit much higher activities than pure Ag₃PO₄ and binary heterostructures of Ag@Ag₃PO₄. The higher photocatalytic activity of the Ag@Ag₃PO₄@ZnO composites may be attributed to the effective photogenerated charge separation at heterointerfaces of Ag/Ag₃PO₄ and Ag₃PO₄/ZnO, and the rapid electron transport along one-dimensional Ag and ZnO nanorods.

© 2015 Elsevier Inc. All rights reserved.

* Corresponding authors at: Department of Chemistry, Tongji University, Siping Road 1239, Shanghai 200092, People's Republic of China. Fax: +86 021 65988029 0 (J. Yang).

E-mail addresses: lilyqin@tongji.edu.cn (Y. Qin), yangjinhu2010@gmail.com (J. Yang).

1. Introduction

Recently, as a new class of semiconductor which can well absorb visible light in solar spectra, Ag₃PO₄ has attracted great attention in photocatalysis field. It is reported that Ag₃PO₄ has

extremely high photo-oxidative capabilities for O₂ evolution from water as well as for organic dye degradation under visible light irradiation, and is able to achieve a quantum efficiency of 90% at wavelengths longer than 420 nm, significantly higher than previously reported values [1,2].

So far, Ag₃PO₄ crystals with a variety of shapes and morphologies such as rhombic dodecahedrons, cubes and spheres have been prepared by Ye and co-workers through a co-precipitation solution method. These Ag₃PO₄ polyhedral/spherical crystals show interesting morphology-related higher photocatalytic activities than traditional N-doped TiO₂ catalysts under visible-light irradiation [3,4]. However, the photocatalytic activity of pure Ag₃PO₄ may still be restricted by its relatively low separation/transportation efficiency of photogenerated charges and limited light harvesting abilities. Previous reports proved that, integrating the objective semiconductor with properly selected metals [5,6] or semiconductors [7,8] to form specific heterostructured composites, can effectively adjust energy band structure and surface charge distribution of the composites and thus improve their overall photoelectric property. Recently our group also reported that the novel metal/oxide semiconductor heterostructures, such as fluffy worm-like Ag core nanowires (NWs)-ZnO branched nanorods (ZnO BNRs) [9] and dandelion-like Au core nanoparticles (NPs)-ZnO nanorods (ZnO NRs) heterostructures [10], showed enhanced photocatalytic properties than pure ZnO nanorods, due to their heterogeneous features as well as the specially designed architectures.

Thereby, lately Ag₃PO₄-based heterogeneous photocatalysts have received considerable interest. For example, Bi and coworkers have realized selective growth of metallic Ag nanocrystals on Ag₃PO₄ submicro-cubes [11] and selective growth of Ag₃PO₄ submicro-cubes on Ag nanowires [12] to fabricate Ag-Ag₃PO₄ composite photocatalyst with specific architectures, both of which exhibit structure-relevant better photoactivities than pure Ag₃PO₄. Moreover, Ag₃PO₄-based binary heterostructured photocatalysts such as AgX/Ag₃PO₄ [13–14], Ag₃PO₄/In(OH)₃ [15], Ag₃PO₄/Bi₂WO₆ [16] and Graphene oxide (GO)/Ag₃PO₄ [17], have been prepared to either facilitate the separation of photoexcited electron-hole pairs or enhance the light absorption and the stability of the catalyst.

Compared to two-component heterostructures, three-component heterostructured photocatalysts by rationally integrating proper components are more likely to satisfy the requirements for high-efficiency photocatalysts. However, they are apparently more challenging to be fabricated, especially those with specific spatial configurations. To date, only several Ag₃PO₄-based ternary structures including Ag₃PO₄/AgBr/Ag [18], Ag@Ag₃PO₄@Ag₂S [19] and Fe₃O₄@Ag₃PO₄/AgCl [20] have been reported. Herein, we integrate a noble metal (silver) and a large-band-gap semiconductor (ZnO) with Ag₃PO₄ to form one-dimensional (1D) coaxial cable-like structured Ag@Ag₃PO₄@ZnO ternary composites via a three-step seeded growth method for photocatalytic studies. The structure of the ternary composites was characterized and the possible growth mechanism was discussed. Photo-degradation of RhB under 300 W high pressure mercury lamp and solar simulator were chosen to evaluate the catalytic activities of the synthesized composite catalyst. In addition, the influence of the catalyst composition and structures on the catalytic performances has been discussed.

2. Experimental section

2.1. Materials

All reagents are analytical grade. Ethyleneglycol(EG), polyvinylpyrrolidone (PVP, Mw = 58,000, 40,000, 10,000), silver nitrate (AgNO₃), ammonium hydroxide (NH₃·H₂O), zincacetate

(Zn(Ac)₂), Rhodamine B chloride (RhB), ethanol (C₂H₅OH), hexamethylenetetramine (HMT) and zinc nitrate hexahydrate (Zn(NO₃)₂·6H₂O) were purchased from Alfa Aesar (China) Chemical Co. Ltd. Disodium hydrogen orthophosphate (Na₂HPO₄) and sodium sulfide (Na₂S) were bought from Aladdin Industrial Corporation (China). All the materials were used directly without further treatment.

2.2. Synthesis of Ag nanorods [21]

In a typical synthesis process, 6 mL of EG was first added to a 25 mL round-bottom flask followed by fierce stirring at 155 °C for 1 h. Then 6 mL of PVP (Mw = 58,000) solution (0.2 M in EG) was rapidly injected into the flask. After stirring for 10 min, 4 mL AgNO₃ solution (0.13 M in EG) was added drop by drop. The mixed solution was kept at 155 °C for 190 min with continuous stirring, leading to the formation of Ag nanorods. The product was collected by centrifuging at a speed of 5000 r/min and rinsed with acetone and deionized water repeatedly for 3 times. The obtained Ag nanorods were stored and sealed in deionized water before use.

2.3. Synthesis of Ag@Ag₃PO₄ composites [12]

Firstly, 3 mL of PVP (Mw = 40,000, 50 g/L) solution was injected into a tube containing 2.5 mL the as-prepared Ag nanorods suspension. After 30 min, the suspension was centrifuged and rinsed with water to remove the excessive PVP, EG and small nanoparticles before re-dispersed in 3 mL deionized water. Afterwards, 0.15 M aqueous solution containing [Ag(NH₃)₂]⁺ was added under stirring for 15 min, followed by the dropwise addition of 0.15 M aqueous solution of Na₂HPO₄.

2.4. Synthesis of ZnO nanoseeds [9]

ZnO nanoseed solution (ZnO sol) was prepared as reported previously. First, 125 mL of zinc acetate solution in methanol (0.01 M) was prepared. Then, 65 mL of KOH solution in methanol (0.03 M) was injected dropwise. The ZnO sol was obtained after continuous stirring the above mixed solution at 60 °C for 2 h.

2.5. Synthesis of Ag@Ag₃PO₄@ZnO ternary composites

10 ml PVP (Mw = 10,000, 0.1 g/L) solution was added into the prepared Ag@Ag₃PO₄ suspension and kept static for 4 h. Then the solution was centrifuged, washed with water and dried at 60 °C. Subsequently, the sample was dispersed in the prepared ZnO nanoseed solution. After stirring for 3 h, the product was collected by centrifuging and rinsed with water. Finally, the ZnO seed-coated Ag@Ag₃PO₄ heterostructures were added to 30 mL aqueous solution composed of equimolar hexamethylenetetramine (HMT) (0.05 M) and zinc nitrate (0.05 M). After incubation at 85 °C for 3 h, the product was collected from the solution, washed with deionized water, and dried in the air. The synthesis process was further illustrated in Fig. S1.

2.6. Photocatalytic activity measurement

2.6.1. Preparation of glass slide-supported heterogeneous catalyst

0.3 mg of the prepared catalyst was well-dispersed into 2 ml of deionized water under ultrasonic oscillation as a stock solution. 0.8 ml of the stock solution was then spin-coated on a glass slide of 1.5 × 1.5 cm² to be used in the heterogeneous catalysis.

2.6.2. Photocatalysis experiments

The glass slide was immersed in the RhB solution (0.8 mg/L) and kept in dark for about 1 h to reach an adsorption/desorption

equilibrium. The system was then irradiated by a 300 W high pressure mercury lamp or solar simulator under magnetic stirring. After every 10 min, the solution of the photodegradation system was sampled and detected using UV–vis spectroscopy. The degradation of RhB in the solution was estimated by the optical density change of RhB at 554 nm.

2.7. Characterization

Morphology was characterized using a scanning electron microscope (SEM, Hitachi S4800, 3 kV) equipped with associated energy-dispersive X-ray spectroscopy (EDX) and high-resolution transmission electron microscopy (HR-TEM, JEM 2011, 200 kV). The crystal structure was determined by X-ray diffraction (XRD) using a D/max2550VB3+/PC X-ray diffractometer with Cu K α radiation with a 1.5418 Å wavelength. A beam voltage of 40 kV and a 100 mA current beam were used. The UV–vis spectra of the samples were recorded on a UV–vis diffuse reflectance spectrometer (InstantSpec BWS003) with an integrating sphere accessory. Photoluminescence (PL) spectra were measured by a LS-55 fluorescence spectrophotometer with the excitation wavelength of 367 nm, the scanning speed of 500 nm/min and the width of excitation slit of 10 nm.

3. Results and discussion

As shown in Fig. 1, the ternary heterostructures were fabricated via a three-step strategy involving Ag₃PO₄ crystal deposition, ZnO seed coating and heteroepitaxial growth processes. To be specific, Ag nanorods fabricated via a modified polyol method [21] serve as the substrates for subsequent Ag₃PO₄ deposition in an aqueous solution containing mainly [Ag(NH₃)₂]⁺ and HPO₄²⁻ (I). Notably, in this step, PVP plays a key role as the bridging molecule to effectively decrease the high interfacial energy between Ag nanorods and Ag₃PO₄ nanoparticles [22]. Otherwise, Ag₃PO₄ would preferentially nucleate in the solution rather than on the surfaces of Ag nanorods. Moreover, due to this PVP-assisted templating method, the hetero-grown Ag₃PO₄ crystals in our work are smaller in size than those reported in previous work [3] and are distributed evenly on the surfaces of Ag nanorods, which are favorable for enhanced light absorption and molecule adsorption. ZnO seeds were deposited on the surfaces of Ag@Ag₃PO₄ simply by immersing the PVP modified Ag@Ag₃PO₄ in the ZnO-nanoseed sol with stirring (II). Then, ZnO nanorod arrays were epitaxially grown on the surface of Ag₃PO₄ via a seed-mediated growth process, leading to the formation of Ag@Ag₃PO₄@ZnO ternary heterostructures (III) [10].

Fig. 2 shows the SEM images of the prepared samples at different preparation stages. The Ag nanorods which serve as non-planar

substrates with smooth surface are ~10 μ m in length and 150 nm in diameter. After Ag₃PO₄ crystal deposition, the surface of Ag nanorods gets rough (Fig. 2b and c). When adjusting the reactant concentrations (see Fig. S2) to 0.15 M (standard condition), the deposited Ag₃PO₄ crystals are polycrystalline nanoparticles arranging continuously along the Ag nanorods with a proper density. This is different from Bi's work [12], where Ag₃PO₄ coatings either in a nearly amorphous phase cover the surface of Ag nanorods completely or in the form of micron-sized single crystalline particles are strung along the Ag nanowires with relatively large inter-particle distance of ~several hundred nanometers. Compared with the above referred Ag/Ag₃PO₄ heterostructures, Ag@Ag₃PO₄ heterostructures prepared in current work with the dense coverage of crystalline Ag₃PO₄ particles on Ag core nanorods may be more efficient for both light absorption and photoinduced charge separation and transport in photocatalysis applications. By adjusting the concentrations of HMT and zinc nitrate (see Fig. S3), ZnO nanorod arrays grown perpendicular to the surface of Ag@Ag₃PO₄ heterostructures were obtained, i.e., the Ag@Ag₃PO₄@ZnO ternary heterostructures (Fig. 2d–f). Although ZnO nanorods are not well-distributed, which may be ascribed to the rough surface of 1D Ag@Ag₃PO₄ hybrid rods, this non-uniformity endows the product with relatively good translucency as well as large specific surface area for light harvesting.

X-ray diffraction (XRD) analysis was explored to examine the crystal structures of the obtained samples. As shown in Fig. 3C, the peaks of the XRD pattern for Ag nanorods can be indexed to face-centered cubic phase of pure Ag (JCPDS, No. 04–0783) [21]. Fig. 3B is the XRD pattern of Ag@Ag₃PO₄ composites. Except for the peaks belong to Ag nanorods, the other peaks in Fig. 3B marked with pink inverted triangle can be indexed to Ag₃PO₄ (JCPDS, No. 06–0505) [3]. And it is notable that compared to Fig. 3C, the intensity of those peaks belonging to Ag decreases drastically, indicating the dense deposition of Ag₃PO₄ on the Ag nanorods. In the case of the Ag@Ag₃PO₄@ZnO ternary heterostructures, there are three groups of diffraction peaks which can be assigned to Ag, Ag₃PO₄ and ZnO (marked with red inverted triangles, JCPDS, No. 36–1451) [10], respectively. Moreover, the energy dispersive spectroscopy (EDS) (Fig. S4) of the Ag@Ag₃PO₄@ZnO heterostructures also indicates the existence of Ag, P, O and Zn elements, aside from the Si signal coming from the silicon substrate used for EDS analysis and the C signal from the residual PVP molecules, which further confirms the ternary composition of our target product.

The optical properties of the obtained samples were studied using UV–vis diffuse reflectance spectra (DRS) and shown in Fig. 4. For comparison, the DRS of pure Ag₃PO₄ sub-micro-cubes prepared according to reference [3] was also provided. As reported [23], pure Ag₃PO₄ can absorb visible light shorter than 530 nm in wavelength (the magenta curve in Fig. 4). For the Ag@Ag₃PO₄



Fig. 1. Schematic illustration of the growth process of Ag@Ag₃PO₄@ZnO ternary heterostructures.

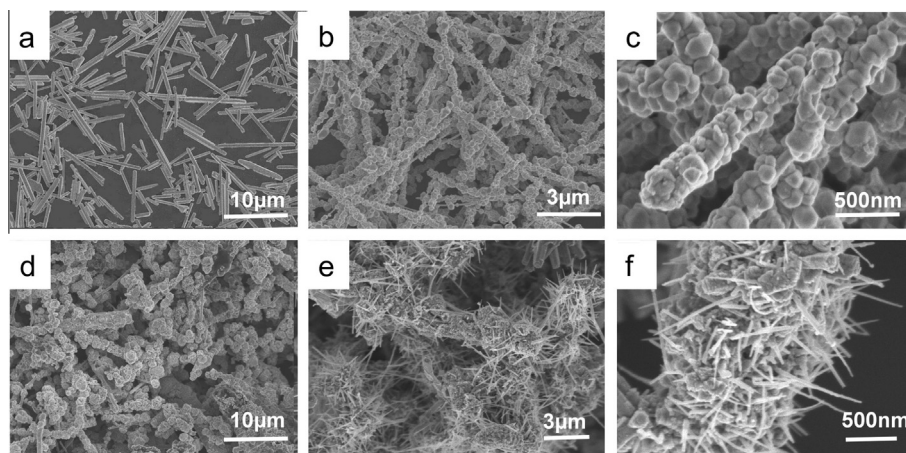


Fig. 2. SEM images of Ag nanorods (a), Ag@Ag₃PO₄ (b and c), and Ag@Ag₃PO₄@ZnO ternary heterostructures (d–f).

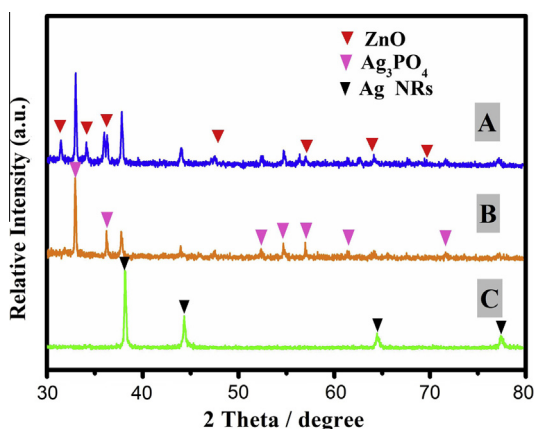


Fig. 3. XRD patterns of (A) Ag@Ag₃PO₄@ZnO ternary heterostructures, (B) Ag@Ag₃PO₄ binary heterostructures and (C) Ag nanorods.

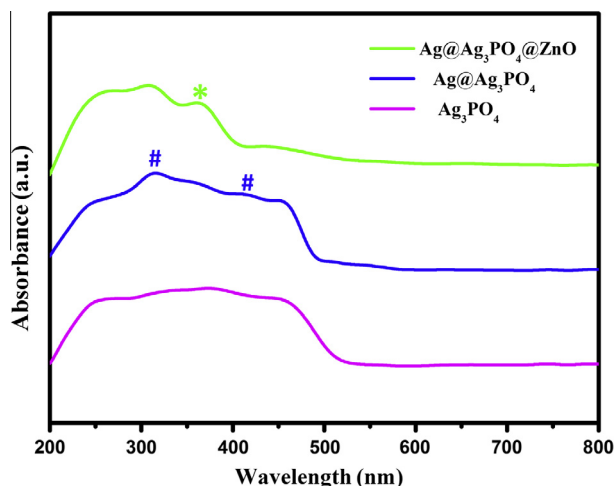


Fig. 4. UV-vis diffuse-reflectance spectra of Ag₃PO₄ crystals, Ag@Ag₃PO₄ binary heterostructures and Ag@Ag₃PO₄@ZnO ternary heterostructures.

binary heterostructures in current work, besides the absorption peaks ascribed to Ag₃PO₄, two new peaks centered at about 320 and 420 nm (marked with pound sign, the blue curve in Fig. 4) are appeared. The former one could be indexed to the directly bonding of electrons to the silver atoms in bulk silver [24], and

the latter is due to the unique surface plasmon resonance (SPR) absorption of Ag nanorods. For the Ag@Ag₃PO₄@ZnO ternary heterostructures, it is obvious that their absorption band entirely overlaps that of pure Ag₃PO₄. However, the ultraviolet absorption region (200–400 nm) of the ternary heterostructures is prominently intensified with the two absorption peaks centered at ~320 and ~370 nm corresponding to the electron binding of Ag and the typical band absorption of ZnO (marked with a star in the green curve) [25]. This reveals that integration of Ag and ZnO with Ag₃PO₄ can greatly enhance the light harvesting ability of the composites especially in the ultraviolet region. Furthermore, the three components of Ag, Ag₃PO₄ and ZnO possess a good match in their energy band structure, for example, their band-edge positions: ZnO (CB = -0.6 eV, VB = 2.6 eV) [26], Ag₃PO₄ (CB = 0.45 eV, VB = 2.88 eV) [18] and Ag (Ef Ag = 0.4 eV vs. normal hydrogen electrode (NHE)) [22]. Therefore, as illustrated in Fig. 5a and b, due to the coaxial structure and the matched energy band-edge of the three components, photo-generated electrons can readily transfer to and concentrate on the surface of Ag nanorods, while the holes transport to the valence band of ZnO, thus decreasing the recombination rate of the photo-induced charge carriers. Moreover, photoluminescence (PL) emission spectra of the samples were also recorded to obtain more information about the surface vacancies and migration and separation of the photo-induced charge carriers. The PL spectra of the pure Ag₃PO₄ sub-micro-cubes and the Ag@Ag₃PO₄ and Ag@Ag₃PO₄@ZnO heterostructures are demonstrated in Fig. S5. For pure Ag₃PO₄, the broad PL emission peak centered at 480 could be attributed to the recombination of the photo-generated charge carriers between the O2p orbit and the empty d orbit of the central Ag⁺ or of the self-trap excitons in the PO₄ oxyanion complex, while the peak centered at 500 nm is considered to originate from the recombination of photo-generated holes with electrons around the surface oxygen vacancies [24]. Compared with pure Ag₃PO₄, the PL spectra of Ag@Ag₃PO₄ and Ag@Ag₃PO₄@ZnO composites have similar emission peaks in the test range. Notably, for the Ag@Ag₃PO₄@ZnO ternary heterostructures, the peak centered at 500 nm almost vanishes, indicating that integration of Ag and ZnO with Ag₃PO₄ in a core-shell structure is very favorable to separate the photogenerated charge carriers and inhibit their recombination, thus leading to the quenching of PL emission.

The photocatalytic performances of the obtained samples were evaluated by degradation of RhB under ultraviolet-visible light irradiation (Fig. 6). For comparison, degradation experiments without catalyst or using pure Ag₃PO₄, and the Ag@Ag₃PO₄ binary heterostructures as the catalysts were also conducted respectively.

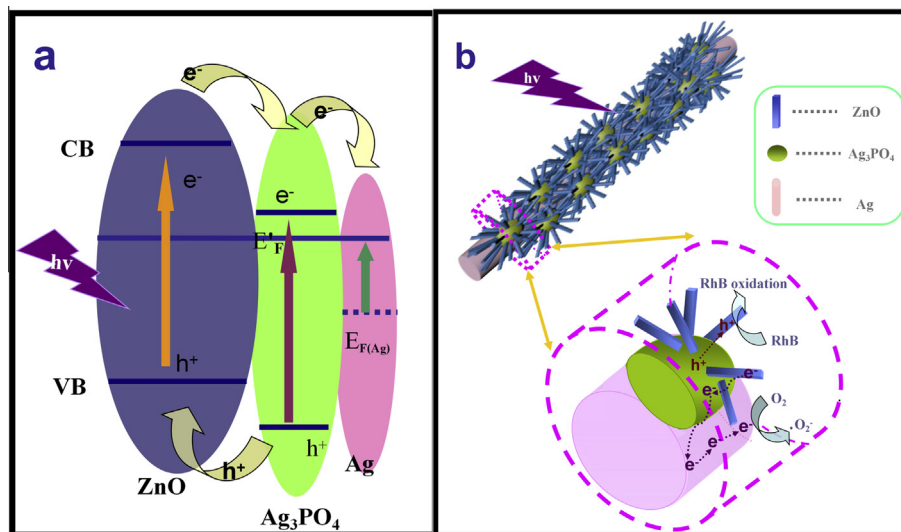


Fig. 5. Schematic diagrams of the energy band structures (a) and photocatalytic reaction process (b) for Ag@Ag₃PO₄@ZnO ternary heterostructured photocatalyst.

It is noted that all the samples (~ 0.12 mg, the standard weight in current catalytic system (see Fig. S6)) were deposited on 1.5×1.5 cm² coverslips and immersed face-up in the solution of RhB under irradiation of a high pressure Hg lamp. According to the photodegradation curves shown in Fig. 6, the photocatalytic efficiency of the studied catalysts follows the order: Ag@Ag₃PO₄@ZnO (green) > Ag@Ag₃PO₄ (magenta) > Ag₃PO₄ (Cyan) > Blank (blue, no catalyst added). Combined with the light absorption properties (Fig. 4) and the energy band structures of the catalysts (Fig. 5a), the above photocatalytic performance order can be explained as follows: (1) It is well-reasoned that the degradation rate is faster when using Ag₃PO₄ as the catalyst than that with no catalyst added, because Ag₃PO₄, a narrow-band semiconductor (2.43 eV), has been proved to be a good catalyst under visible-light irradiation [18]. (2) The integration of Ag with Ag₃PO₄, for one thing, could enhance the light absorption ability of Ag₃PO₄ as demonstrated in Fig. 4; for another thing, facilitates the photo-induced charge carrier separation. Thus the Ag@Ag₃PO₄ binary heterostructure has improved photocatalytic performance than pure Ag₃PO₄, which agrees with Bi's reports

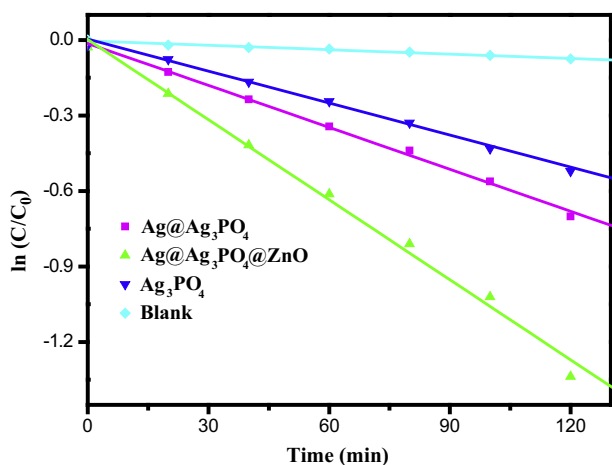


Fig. 6. Photocatalytic degradation of RhB upon different catalysts of pure Ag₃PO₄, binary Ag@Ag₃PO₄, ternary Ag@Ag₃PO₄@ZnO as well as blank respectively under ultraviolet–visible light irradiation at room temperature.

[22]. (3) In the case of the Ag@Ag₃PO₄@ZnO ternary heterostructures, the deposition of ZnO, a wide-band-gap semiconductor (3.2 eV), further enhanced the absorption in UV region, which greatly improved the light harvesting capacity of the heterostructured catalyst. Importantly, the delicately matched band structures of ZnO, Ag₃PO₄ and Ag (Fig. 5a), are very favorable for the excited electrons to transfer from the conduction bands of ZnO and Ag₃PO₄ to the newly rebuilt surface energy band of Ag, leaving holes accumulating in the valence band of ZnO or Ag₃PO₄. Therefore, this ternary heterostructure not only intensifies the light harvesting capacity of the composite catalyst, but also improves the separation and transportation efficiency of the photo-induced charge carriers. (4) Last but not least, the rationally designed heterogeneous architecture of the three-component photocatalyst consisting of the core of 1D Ag nanorods, the interlayer of Ag₃PO₄ crystalline nanoparticle and the outer layer of arrayed ZnO nanorods, with high carrier transportation features, can serve as spatially extended catalyzing centers to provide electrons/holes to the acceptors (O₂, H₂O, RhB) [9] in a direct and timely-supplied way. Fig. 5b was plotted to illustrate the detailed function mechanism of the spatially extended catalyzing centers: upon exciting with light, a fast charge separation and transportation process is initiated, electrons enriched on the Ag nanowires would participate in and facilitate the multiple-electron reduction reaction of oxygen (O₂ + 2H⁺ + 2e⁻ → H₂O₂) [11,27]. Simultaneously, the accumulated holes on ZnO rods and Ag₃PO₄ particles would function as the high-energy oxidants to accelerate the degradation of RhB molecules. Moreover, the hierarchical heterostructured assemblies with fluffy worm-like morphology endow the catalysts with a larger specific surface area and more accessible active sites for improved adsorption and diffusion of molecules involved in the desired photochemical reactions.

Degradation of RhB under solar simulator using the synthesized samples were also conducted as shown in Fig. S7. Different from the results shown in Fig. 6, photocatalytic activities of the studied catalysts under simulated solar light irradiation follows the order of Ag@Ag₃PO₄ > Ag@Ag₃PO₄@ZnO > Ag₃PO₄, which is reasonable when considering that the ultraviolet light content in the solar spectrum is less than 5% while in the mercury lamp spectrum, ultra-violet possesses a large percent. Therefore, although the presence of ZnO enhances the light absorption of Ag in the visible to near-infrared region, the main function of ZnO is harvesting

ultra-violet light and inject excited electrons to Ag_3PO_4 and Ag, thus improving the efficiency of the composite photocatalyst. Since the ultra-violet light content in the solar simulator spectrum is low, the function of ZnO nanorods in the $\text{Ag}@\text{Ag}_3\text{PO}_4@\text{ZnO}$ ternary hetero-structures is very limited. Even worse, the presence of ZnO nanorods may shade and reflect part of the light which should have been absorbed by Ag_3PO_4 and Ag. From this point of view, ternary composite photocatalysts formed by small ZnO nanoparticles, rather than ZnO nanorod arrays, distributed on the surface of $\text{Ag}@\text{Ag}_3\text{PO}_4$ in a proper density may be more favorable for those photocatalytic applications irradiated under solar light. At present, the relevant work is in progress in our group.

4. Conclusions

In summary, we have demonstrated an effective seed-mediated deposition approach to prepare novel fluffy worm-like $\text{Ag}@\text{Ag}_3\text{PO}_4@\text{ZnO}$ ternary heterostructures. The $\text{Ag}@\text{Ag}_3\text{PO}_4@\text{ZnO}$ ternary hetero-structures showed much higher photocatalytic activities than pure Ag_3PO_4 and $\text{Ag}@\text{Ag}_3\text{PO}_4$ binary heterostructures upon UV–visible light irradiation. This could be ascribed to the energy band structure match of the selected components (Ag, Ag_3PO_4 and ZnO) and the rationally designed architectures of the ternary heterostructures, which enabled efficient channeling of the photogenerated charge carriers and therefore led to improved photocatalytic performance, compared to pure or binary photocatalysts. This strategy may also be adapted for preparing other multicomponent heterostructures with promising applications in solar energy conversion, sensing and other photoelectric fields.

Acknowledgments

This work was financially supported by National Natural Science Foundation (21273161 and 21101117), The Program for Professor of Special Appointment (Eastern Scholar) at Shanghai Institutions of Higher Learning, Shanghai Innovation Program (13ZZ026), Scientific Research Foundation for the Returned Overseas Chinese Scholars of SEM and the Fundamental Research Funds for the Central Universities, Foundation for Innovative Research Groups of the National Natural Science Foundation of China (81221001).

Appendix A. Supplementary material

Supplementary data associated with this article can be found, in the online version, at <http://dx.doi.org/10.1016/j.jcis.2015.03.066>.

References

- [1] Z.G. Yi, J.H. Ye, N. Kikugawa, T. Kako, S.X. Ouyang, H. Stuart-Williams, H. Yang, J.Y. Cao, W.J. Luo, Z.S. Li, Y. Liu, R. Withers, *Nat. Mater.* 9 (2010) 559–564.
- [2] Q.H. Liang, W.J. Ma, Y. Shi, Z. Li, X.M. Yang, *Cryst. Eng. Comm.* 14 (2012) 2966–2973.
- [3] Y.P. Bi, S.X. Ouyang, N. Umezawa, J.Y. Cao, J.H. Ye, *J. Am. Chem. Soc.* 133 (2011) 6490–6492.
- [4] Y.P. Bi, H.Y. Hu, S.X. Ouyang, G.X. Lu, J.Y. Cao, J.H. Ye, *Chem. Commun.* 48 (2012) 3748–3750.
- [5] M.A. Gondal, X.F. Chang, W. Sha, Z.H. Yamani, Q. Zhou, *J. Colloid Interface Sci.* 392 (2013) 325–330.
- [6] W. Teng, X.Y. Li, Q.D. Zhao, J.J. Zhao, D.K. Zhang, *Appl. Catal. B: Environ.* 125 (2012) 538–545.
- [7] J.J. Guo, H. Zhou, S.X. Ouyang, T. Kakobc, J.H. Ye, *Nanoscale* 6 (2014) 7303–7311.
- [8] W.C. Peng, X. Wang, X.Y. Li, *Nanoscale* 6 (2014) 8311–8317.
- [9] S.W. Wang, Y. Yu, Y.H. Zuo, C.Z. Li, J.H. Yang, C.H. Lu, *Nanoscale* 4 (2012) 5895–5901.
- [10] Y.H. Zuo, Y. Qin, C. Jin, Y. Li, D.L. Shi, Q.S. Wu, J.H. Yang, *Nanoscale* 5 (2013) 4388–4394.
- [11] Y.P. Bi, H.Y. Hu, S.X. Ouyang, Z.B. Jiao, G.X. Lu, J.H. Ye, *Chem. Eur. J.* 18 (2012) 14272–14275.
- [12] Y.P. Bi, H.Y. Hu, S.X. Ouyang, Z.B. Jiao, G.X. Lu, J.H. Ye, *J. Mater. Chem.* 22 (2012) 14847–14850.
- [13] Y.P. Bi, S.X. Ouyang, J.Y. Cao, J.H. Ye, *Phys. Chem. Chem. Phys.* 13 (2011) 10071–10075.
- [14] J.J. Ren, H. Eckert, *J. Phys. Chem. C* 117 (2013) 24746–24751.
- [15] J.J. Guo, S.X. Ouyang, H. Zhou, T. Kako, J.H. Ye, *J. Phys. Chem. C* 117 (2013) 17716–17724.
- [16] G.K. Fu, G.A. Xu, S.P. Chen, L. Lei, M.L. Zhang, *Catal. Commun.* 40 (2013) 120–124.
- [17] L. Xu, W.Q. Huang, L.L. Wang, G.F. Huang, P. Peng, *J. Phys. Chem. C* 118 (2014) 12972–12979.
- [18] W.S. Wang, H. Du, R.X. Wang, T. Wen, A.W. Xu, *Nanoscale* 5 (2013) 3315–3321.
- [19] J.T. Tang, W. Gong, T.J. Cai, T. Xie, C. Deng, Z.S. Peng, Q. Deng, *RSC Adv.* 3 (2013) 2543–2547.
- [20] X. Guo, N. Chen, C.P. Feng, Y.N. Yang, B.G. Zhang, G. Wang, Z.Y. Zhang, *Catal. Commun.* 38 (2013) 26–30.
- [21] B.J. Wiley, Y. Chen, J.M. McLellan, Y.J. Xiong, Z.Y. Li, D. Ginger, Y.N. Xia, *Nano Lett.* 7 (2007) 1032–1036.
- [22] H.Y. Hu, Z.B. Jiao, T. Wang, J.H. Ye, G.X. Lu, Y.P. Bi, *J. Mater. Chem. A* (2013) 10612–10616.
- [23] Z.B. Jiao, Y. Zhang, H.C. Yu, G.X. Lu, J.H. Ye, Y.P. Bi, *Chem. Commun.* 49 (2013) 636–638.
- [24] Q.H. Liang, Y. Shi, W.J. Ma, Z. Li, X.M. Yang, *Phys. Chem. Chem. Phys.* 14 (2012) 15657–15665.
- [25] T.H. Yang, L.D. Huang, Y.W. Harn, C.C. Lin, J.K. Chang, C.I. Wu, J.M. Wu, *Small* 9 (2013) 3169–3182.
- [26] X.N. Wang, H.J. Zhu, Y.M. Xu, H. Wang, Y. Tao, S.K. Hark, X.D. Xiao, Q. Li, *ACS Nano* 4 (2010) 3302–3308.
- [27] T. Tatsuma, K. Takada, T. Miyazaki, *Adv. Mater.* 19 (2007) 1249–1251.